Optical Materials 95 (2019) 109218

Contents lists available at ScienceDirect

Optical Materials

journal homepage: www.elsevier.com/locate/optmat

Promising PVA/TiO_2, CuO filled nanocomposites for electrical and third order nonlinear optical applications

Gananatha Shetty B[a], Vincent Crasta[b,*], Rithin Kumar N B[c], Rajesh K[b], Raghavendra Bairy[d], Parutagouda Shankaragouda Patil[e]

[a] Department of Physics, Alva's College, Moodbidri, 574227, Karnataka, India
[b] Departmentof Physics, St. Joseph Engineering College, Vamanjoor, Mangaluru, 575028, Karnataka, India
[c] Departmentof Physics, A.J Institute of Engineering and Technology, Mangaluru, 575006, Karnataka, India
[d] Departmentof Physics, NMAM Institute of Technology, Nitte, Karkala, 574110, Karnataka, India
[e] Department of Physics, K.L.E. Institute of Technology, Hubballi, 580030, Karnataka, India

ARTICLE INFO

Keywords:
PVA
Nanocomposites
NLO
Photoluminescence

ABSTRACT

In this paper, we report enhancing the structural, morphological, mechanical, linear and nonlinear optical properties of polyvinyl alcohol (PVA) encapsulated with titanium dioxide (TiO_2) and copper oxide (CuO) nanoparticles. PVA/(x)TiO_2(15-x)CuO nanocomposites for x = 0 wt%, 1 wt%, 5 wt%, 7.5 wt%, 10 wt%, 14 wt% and 15 wt% filling concentration are prepared using ex-situ and solvent casting technique. The XRD spectra of the prepared nanocomposites endorse the semi-crystalline nature of PVA nanocomposites. The atomic force microscope (AFM) image displayed the uniform grain structure for pure PVA and change in surface morphology for prepared nanocomposites. Universal testing machine (UTM) explored high tensile strength and Young's modulus of 1685.70 MPa for x = 10 wt% filling concentration. PVA/(x)TiO_2(15-x)CuO nanocomposites shows an enhanced electrical conductivity of $3.21 \times 10^{-8} Scm^{-1}$ for x = 10 wt% filling concentration. UV–Vis spectroscopy exposed the reduction in optical energy gap with the increase in filling concentration. Photoluminescence (PL) studies spectacles maximum enhancement in PL intensity for x = 10 wt% filling concentration. The Z-scan technique shows third order nonlinear absorption coefficient of 8.17×10^{-4} cm/W, the nonlinear refractive index of $2.56 \times 10^{-8} cm^2/W$ and nonlinear optical susceptibility of 1.48×10^{-6} esu for optimum nanocomposites.

1. Introduction

Of late, scientific as well as technological interests have created a heavy demand for metal oxide polymer nanocomposites [1–3]. These metal oxide polymer nanocomposites encompass relatively small metal oxides of size ranging between 1 and 100 nm dispersed uniformly in a host polymer matrix. The addition of metal oxide nanoparticles into a polymer matrix will advance the properties of the prepared nanocomposites [4–7]. In recent years, PVA arises as an excellent host polymer matrix for filling of nanoparticle due to its high dielectric strength, excellent emulsifying, good charge storing capacity, thin film forming and adhesive properties. This PVA is an atactic material that exhibits crystallinity as well as incompressible properties. Its high oxygen and aromatic barriers with added nanoparticles gives excellent tensile strength and flexibility for the PVA nanocomposites [8–10].

The gain in increasing demand for the search of excellent nanoparticles is a continuous research. In this regard, copper oxide appears to be outstanding metal oxide nanoparticles due to its excellent physical and chemical properties, which finds application in solar cells [11], photodetectors [12], biosensors [13], gas sensors [14] magnetic storage media [15] thermoelectric and photoconductive cells etc. [16–18]. On the other hand, TiO_2 nanoparticle also serves as an excellent filler material in the PVA matrix due to its high surface area, excellent transparency, good stability and its ability to inhibit bacterial growth there by retaining the physical and chemical properties of the nanocomposites [19–21]. TiO_2 is an important global product with many applications related to electronics, photonics, cosmetic items, sunscreen lotions, water treatment agents, printing inks, textiles, paints and ceramics etc. [22].

PVA predicted polymer nanocomposites with different metal oxide nanoparticle distribution shows enhancement of electrical, mechanical, thermal and NLO properties [23–24]. It was studied PVA/(x)$AgNO_3$(15-

* Corresponding author.
E-mail address: vincentc@sjec.ac.in (V. Crasta).

https://doi.org/10.1016/j.optmat.2019.109218
Received 20 February 2019; Received in revised form 25 May 2019; Accepted 20 June 2019

x)$MnCl_2$ nanocomposites and reported that the shape and special distribution of the mixed fillers are significant aspects in controlling the electrical, optical, thermal and electron spin resonance properties of the polymer system [25]. Recently it was reported that the addition of ZnO and WO_3 nanoparticles into PVA matrix increases the degree of crystallinity due to secondary bonding, this in turn increases the stiffness and strength of PVA [26]. Recently we studied PVA/(x)TiO_2(15-x) MoO_3 nanocomposites and repoted that addition of TiO_2 and MoO_3 nanoparticles into PVA matrix advances the mechanical, electrical and optical properties of the PVA due to their high interfacial interaction between the organic moieties and inorganic nanoparticles [27]. With this interest we have presented the preparation of the polymer nanocomposites using basic host PVA matrix (PVA-MOWIOL 10–98) by filling preferred amount of Titanium dioxide (TiO_2) and Copper oxide (CuO) nanoparticles. The prepared nanocomposites of PVA/(x)TiO_2(15-x)CuO for x = 0, 1, 5, 7.5, 10, 14 and 15 wt% filling concentration alters the molecular and atomic states, resulting unexpected outcomes in structural, mechanical and optical such as photoluminescence, linear, non-linear properties etc.

2. Experimental details

2.1. Preparation of titanium oxide nanoparticles

Titanium oxide nanoparticles were prepared with the following procedure: 20 ml of absolute ethyl alcohol is added to 8 ml of dibutyl phthalate (solution 1) and is kept in a magnetic stirrer for an hour at constant stirring rate of 500 rpm. Second solution is prepared by dissolving 15 g of ammonium titanyl sulphate with 60 ml of de-ionized water and 6 ml of hydrochloric acid. Then both the solutions were mixed together and stirred at 500 rpm using magnetic stirrer until a clear solution is attained. The clear solution is heated up to 95 °C to convert it into a turbid form. Ammonium is added dropwise to the turbid solvent until the solution turns milky white and is allowed to deposit for a day. The filtrate at the bottom is washed with deionising water repeatedly till the pH of the solution turns neutral. Using 0.1 μm Whatman Nylon filter membrane, the neutral residue is filtered and is dried at 550 °C for 2 h to get titanium oxide nanoparticles [28].

2.2. Preparation of CuO nanoparticles

1 ml of the glacial acetic acid solution is mixed with 0.02 mol aqueous solution of copper acetate and the mixture is kept in temperature controlled mechanical stirrer at a stirring rate of 500 rpm and 110 °C temperature for 1 h. To the above mixture 1 M solution of NaOH is added dropwise until a black precipitate of CuO is formed and the same is separated by centrifuging. The precipitate is then washed with deionising water to remove all the traces of NaOH. The achieved CuO is kept in an oven for 8 h at 500 °C which yields around 94%.

2.3. PVA nanocomposites sample preparation

8 g of PVA (MOWIOL 10–98, Sigma Aldrich Germany) is liquefied into a clear viscous solvent by dissolving with distilled water(180 ml) kept in a temperature controlled (80 °C) mechanical stirrer with stirring rate 1200 rpm. Further, PVA solvent is reduced to lab temperature by maintaining the stirring rate at 250 rpm. Divide the solvent into 8 equal parts. TiO_2 and CuO nanoparticles are then filled to each part of PVA solvent as PVA/(x)TiO_2(15-x)CuO for x = 0, 1, 5, 7.5, 10, 14 and 15 wt %. The filled PVA solvent is sonicated using ultrasonicator for 15 min and transferred into a Petri dish. The Petri dish is kept in a muffle furnace at 50 °C for 24 h s. The prepared PVA nanocomposites are then peeled off from the petridish and kept in vacuum desiccators for further study. The film thicknesses were recorded using a dial thickness gauge (Mitutoya, Japan).

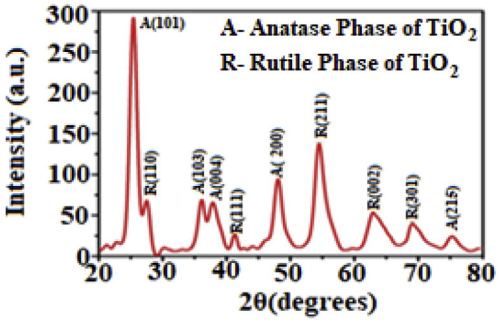

Fig. 1. XRD spectra of pure synthesised TiO_2 nanoparticles.

3. Results and discussion

3.1. XRD studies of TiO_2, CuO and filled PVA nanocomposites

The structural and crystallographic confirmations of prepared nanoparticles of TiO_2, CuO and filled PVA nanocomposites were done using Bruker D_8 Advance X-ray diffractometer (XRD) with Nickel filtered CuKα radiation of wavelength 1.5406 Å. Fig. 1 epitomizes the XRD spectra of pure TiO_2 nanoparticles having embedded peaks at 2θ = 25.44, 36.16, 47.91, 54.43 and 63.4 representing the anatase phase of TiO_2 nanoparticles for planes (101), (103), (004), (200), (105) and (204) respectively. Apart from these, the peaks at 27.47, 41.20, 56.62 and 69.35 denote the rutile phase of TiO_2 nanoparticles for planes (110), (111), (220) and (301) respectively (JCPDS no.: 21–1272 and 21–1276) [29,30].

Fig. 2 shows the Bragg's reflection of CuO nanoparticles. The diffraction peaks at 2θ = 32.58, 35.53, 38.68, 48.93, 53.46, 58.18, 61.72, 66.26, 68.23, 72.56 and 75.12 conforming to its crystal plane (110), (−111), (111), (−202), (020), (202), (−113), (022), (220), (311) and (004) respectively (JCPDS card files no.:48–1548) [31,32].

The confirmation of PVA/(x) TiO_2 (15-x) CuO nanocomposites for x = 0, 1, 5, 7.5, 10, 14 and 15 wt% filling concentrations are witnessed from the peaks of added filler nanoparticle as shown in Fig. 3. The broad as well as widened semi-crystalline peaks at 2θ = 19 to 20^0 corresponds to host PVA main chain. The enhancement in the crystalline nature of PVA nanocomposites is due to the interfacial contacts between the organic PVA-OH group and inorganic nanoparticles phases thereby retaining the intercalation of high molecular weight polymer chains with filled nanoparticles. The intensity of diffraction peak along with the PVA filled nanoparticles proliferates from x = 0 wt% to x = 10 wt% concentration. The intensification in the diffraction peaks of PVA ranging between 19 to 20^0 by the filled nanoparticles, increases the percentage crystallinity of PVA/(x)TiO_2(15-x)CuO for x = 0, 1, 5, 7.5, 10, 14 and 15 wt% nanocomposites. Thus, observed crystallinity

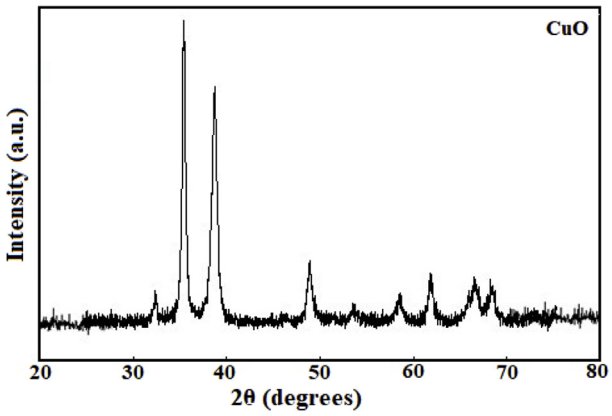

Fig. 2. XRD spectra of pure synthesised CuO nanoparticles.

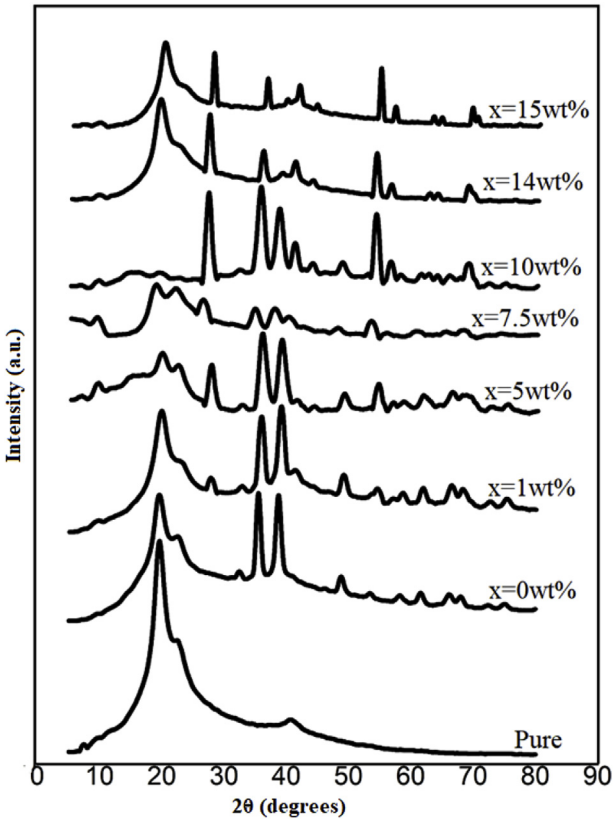

Fig. 3. XRD spectra of PVA/(x)TiO_2 (15-x) CuO for x = 0, 1, 5, 7.5, 10, 14 and 15 wt% filling concentration.

for the doping concentration x = 10 wt%of the PVA nanocomposites depends on the geometrical structure, chemical nature, and homogenous distribution of the Nano filler. On the other hand, by the addition of nanoparticles to the molten PVA at high temperature, the random coils in the PVA start to melt and interpenetrate each other in the form of segmental or molecular motion. This disordered viscous solution of PVA coagulates with the added Nanofillers. Further, the decrease in thermal energy reduces the molecular motion and random coils start to solidify thereby enhancing the crystallinity forming a complex conformation.

3.2. Surface topography using AFM

The Bruker (nano) Atomic Force Microscope (AFM) is used to analyse modification in the size, and uniform dispersion of nanofillers inside the host PVA matrix. The two dimensional (2D) AFM images of pure PVA shown in Fig. 4 (a) specifies the uniform grain structures of

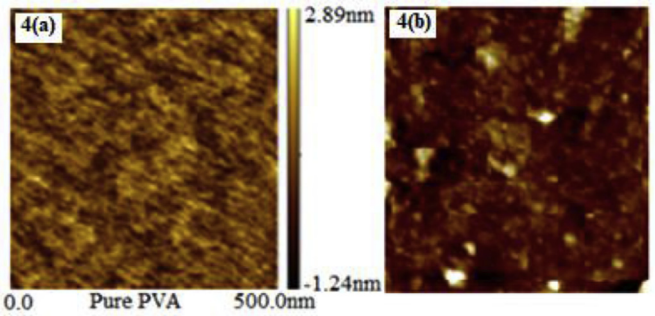

Fig. 4. (a). AFM 2-D images of Pure PVA and Fig. 4(b). PVA/(x)TiO_2(15-x)CuO for x = 10 wt% filling concentration.

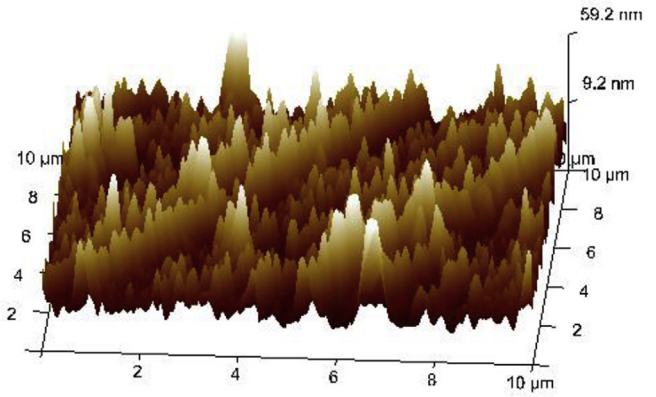

Fig. 5. AFM 3-D images of PVA/(x)TiO_2 (15-x) CuO for x = 10 wt% filling concentration.

pure PVA and Fig. 4(b) spectacles the changes in surface morphology of x = 10 wt% optimized concentration of particle filled nanocomposites. Three dimensional (3D) AFM image of x = 10 wt% optimized filling concentration shown in Fig. 5 signifies no large scale particle agglomeration. The observed parameters such as average surface roughness R_{ave} = 4.46 nm (For pure PVA R_{ave} = 1.15 nm) and RMS surface roughness R_{rms} = 6.39nmfor optimized filling concentration x = 10 wt % compared to pure PVA R_{rms} = 2,82 nm suggests the enhancement in the crystallinity.

3.3. Mechanical studies

The Universal Testing Machine (LLOYD LRX Plus-5 KN, London, UK) is employed for determining the Young's modulus, tensile strength, and stiffness, of the prepared PVA/(x)TiO_2(15-x)CuO for x = 0, 1, 5, 7.5, 10, 14 and 15 wt% nanocomposites. Fig. 6 explores the Stress-Strain curves and Table 1 highlights the mechanical properties of the prepared PVA nanocomposites of different filling concentration at room temperature. The observed high values of Young's modulus 1685.70 MPa, tensile strength 48.36 MPa, and stiffness 33.94 kN/m for optimized doping concentration x = 10 wt% is mainly due to the enhancement in crystallinity as aforementioned in above discussions. The complex conformation of added Nano fillers of optimized doping concentration of 10 wt% forms a high order oriented chain aggregates in the crystalline region providing the immense strength to the nanocomposites. This may also happens due to the plasticizing effects of gallaries, dangling chain formation and also by conformational effects

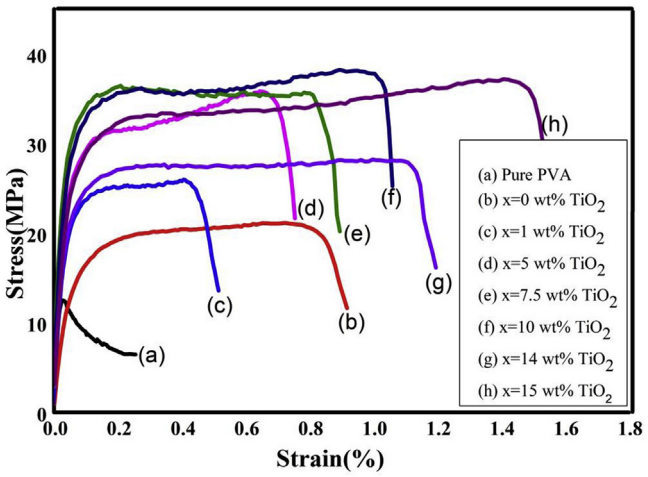

Fig. 6. Stress- Strain curves of PVA/(x)TiO_2(15-x)CuO for x = 0, 1, 5, 7.5, 10, 14 and 15 wt% filling concentration.

Table 1
Mechanical properties of PVA/(x) TiO_2 (15-x) CuO for x = 0, 1, 5, 7.5, 10, 14 and 15 wt% filling concentration.

Dopant Concentration	Tensile Strength (MPa)	Stiffness (kN/m)	Young's Modulus (MPa)	Percentage Total Elongation at Fracture
Pure PVA	2.90	5.34	45.34	32.53
0 wt%	26.85	32.02	421.39	76.23
1 wt%	36.45	33.71	678.92	90.37
5 wt%	31.18	52.67	832.26	92.65
7.5 wt%	35.85	28.14	915.01	107.07
10 wt%	48.36	33.94	1685.70	111.97
14 wt%	42.45	33.29	1125.78	120.77
15 wt%	37.19	33.91	847.84	156.71

Table 2
DC conductivity of PVA/(x) TiO_2 (15-x) CuO for x = 0, 1, 5, 7.5, 10, 14 and 15 wt% filling concentration.

Dopant Concentration	Resistance (Ω)	Conductivity (Scm^{-1})
Pure PVA	0.237×10^9	8.42×10^{-10}
0 wt%	0.563×10^8	7.16×10^{-9}
1 wt%	0.499×10^8	8.02×10^{-9}
5 wt%	0.378×10^8	1.32×10^{-8}
7.5 wt%	0.269×10^8	1.86×10^{-8}
10 wt%	0.249×10^8	3.21×10^{-8}
14 wt%	0.274×10^8	2.19×10^{-8}
15 wt%	0.579×10^8	8.64×10^{-9}

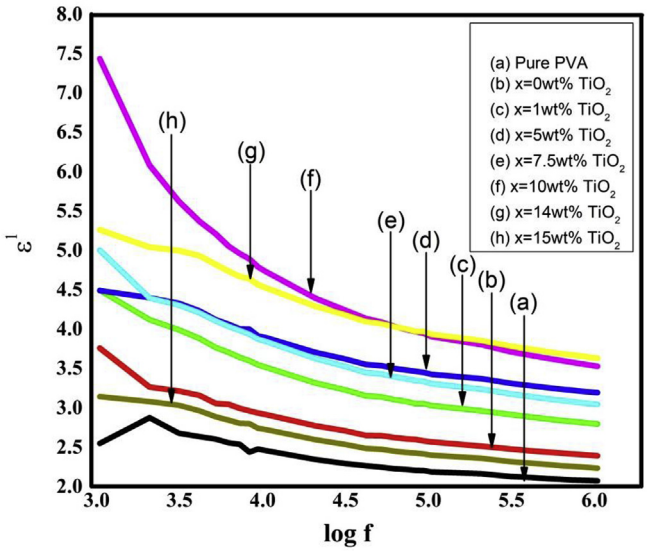

Fig. 7. Variation of dielectric constant with frequency for different doping concentration of PVA nanocomposites.

at the added nanoparticles-PVA interfaces [33]. This combination of improved Young's modulus, its toughness and elasticity make the PVA/(x)TiO_2(15-x)CuO nanocomposites a high performance material. Above x = 10 wt%, due to the formation of exfoliated aggregates and less degree of crystallinty makes the PVA/(x)TiO_2(15-x)CuO nanocomposites to be more brittle, there by decreasing its mechanical properties.

3.4. DC conductivity

Using Keithley 4200-SCS parameter analyser with two probe method at room temperature I–V characteristics of the prepared PVA/(x)TiO_2(15-x)CuO for x = 0, 1, 5, 7.5, 10, 14 and 15 wt% filling nanocomposites were done in the voltage range of 0–20 V. The resistance (R) of prepared nanocomposites obtained from the I–V characteristics is

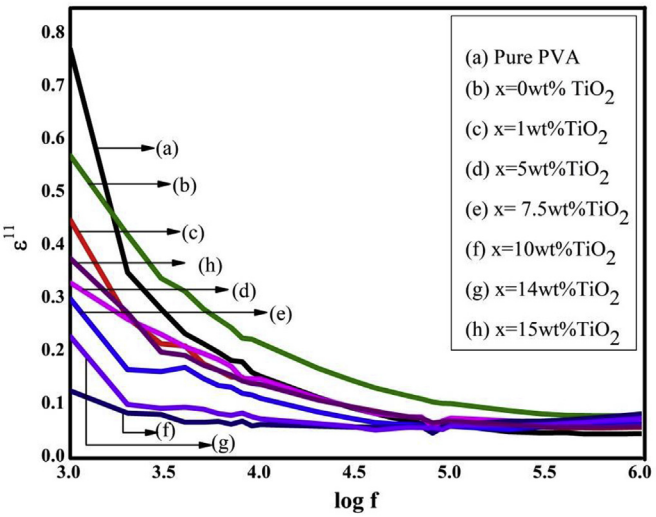

Fig. 8. Dielectric loss with frequency for different doping concentration of PVA nanocomposites.

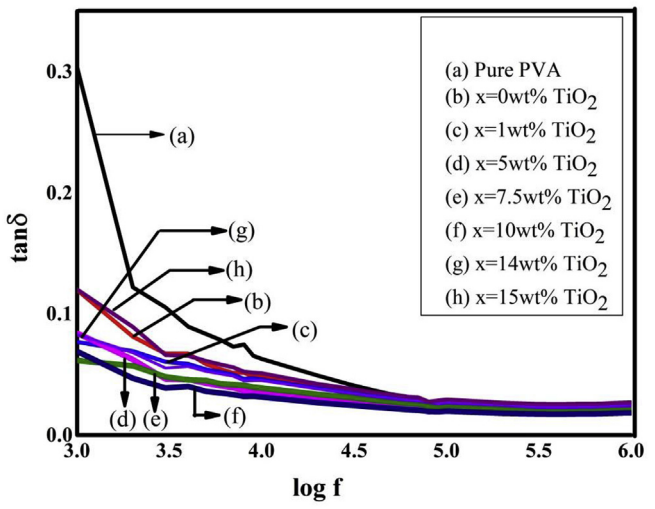

Fig. 9. The dependence of loss factor with change in frequency for different doping concentration of PVA nanocomposites.

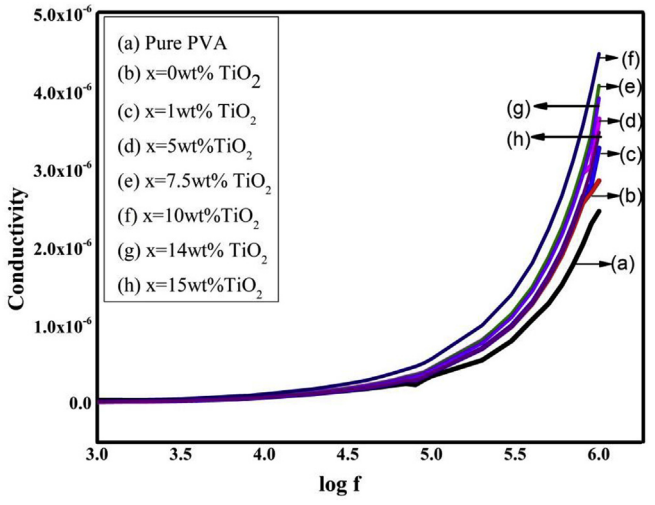

Fig. 10. Dependence of AC conductivity as a function of different dopant concentration of PVA nanocomposites.

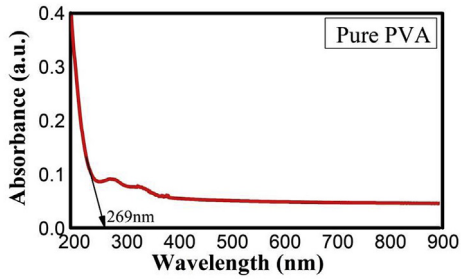

Fig. 11. UV–Visible absorption spectra of pure PVA.

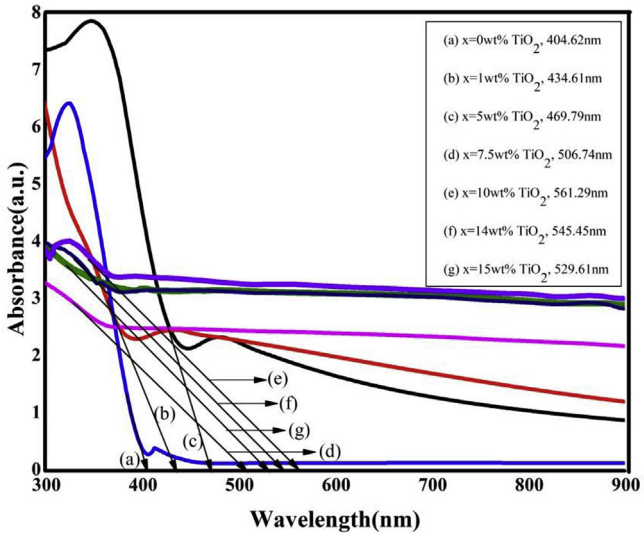

Fig. 12. UV–Visible spectra of PVA/(x)TiO_2(15-x)CuO for x = 0, 1, 5, 7.5, 10, 14 and 15 wt% filling concentration.

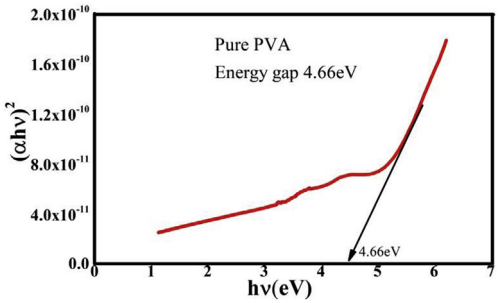

Fig. 13. Optical energy gap of pure PVA.

substituted in the equation $\sigma_{dc} = \frac{d}{RA}$ where'd' is the thickness of polymer nanocomposites, 'A' is the cross-sectional area of electrode, gives the DC conductivity of the prepared nanocomposites. Table 2 exemplifies the resistance and conductivity of prepared PVA nanocomposites of different filling concentrations and it displays a reduction in resistance from x = 0 wt% to x = 10 wt% filling concentration with an enhancement in conductivity. The improvement in the conductivity is due the added mixed fillers of TiO_2 and CuO nanoparticles reside in interstitial sites of PVA main chain due to hopping of charges. Apart from these, the increase in crystallinity also supports charge transfer by reducing the barrier height leading to enhancement in conductivity.

3.4.1. Dielectrics studies

The frequency dependence of the dielectric permittivity (ε′) and capacitance of PVA/(x)TiO_2 (15-x)CuO nanocomposites for x = 0, 1, 5, 7.5, 10, 14 and 15 wt% filling concentrations at room temperature were

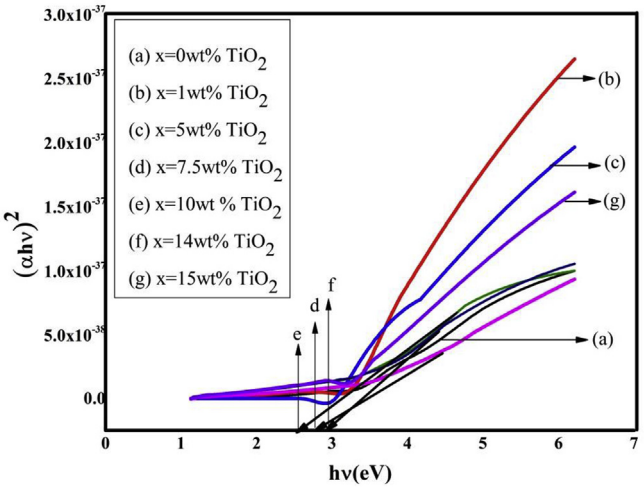

Fig. 14. Optical energy gap of PVA/(x)TiO_2(15-x)CuO for x = 0, 1, 5, 7.5, 10, 14 and 15 wt% filling concentration.

Table 3
Energy band gap of PVA/(x) TiO_2 (15-x) CuO for various filling concentration.

Dopant Concentration	Band gap (eV)
Pure PVA	4.66
0 wt%	3.17
1 wt%	2.99
5 wt%	2.79
7.5 wt%	2.70
10 wt%	2.44
14 wt%	2.95
15 wt%	2.73

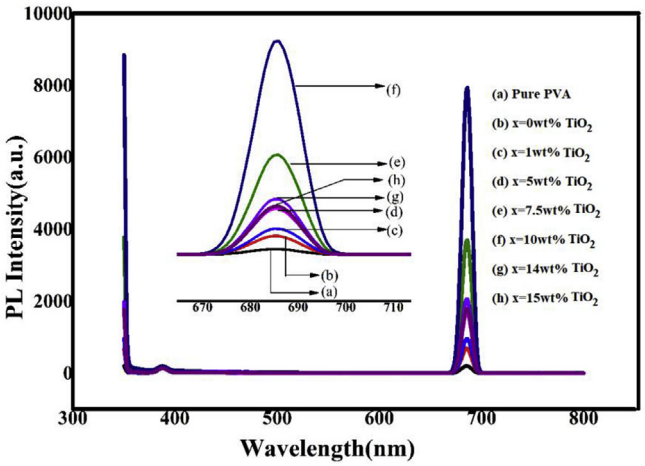

Fig. 15. PL spectra of pure and doped nanocomposites with excitation wavelength 340 nm.

studied using of Keithley 4200-SCS parameter analyser frequency ranging from 1 kHz to 1 MHz. From Fig. 7, one could notice the variation of dielectric constant (ε′) with the increasing frequency. The high dielectric constant at low frequency verifies the polar nature of dielectric molecules [34–37]. At higher values of frequency dipoles will not rotate sufficiently, so that their oscillation will lags behind that of the field. Hence at high frequencies dielectric constant approaches a limit value [38]. Fig. 7 also specifies that at low frequencies all the nanocomposites showed relatively high dielectric permittivity and decreases with the rise in frequency. The fall of polarizability in addition to the occurrence of absorption of electrical energy constituting dielectric dispersion is

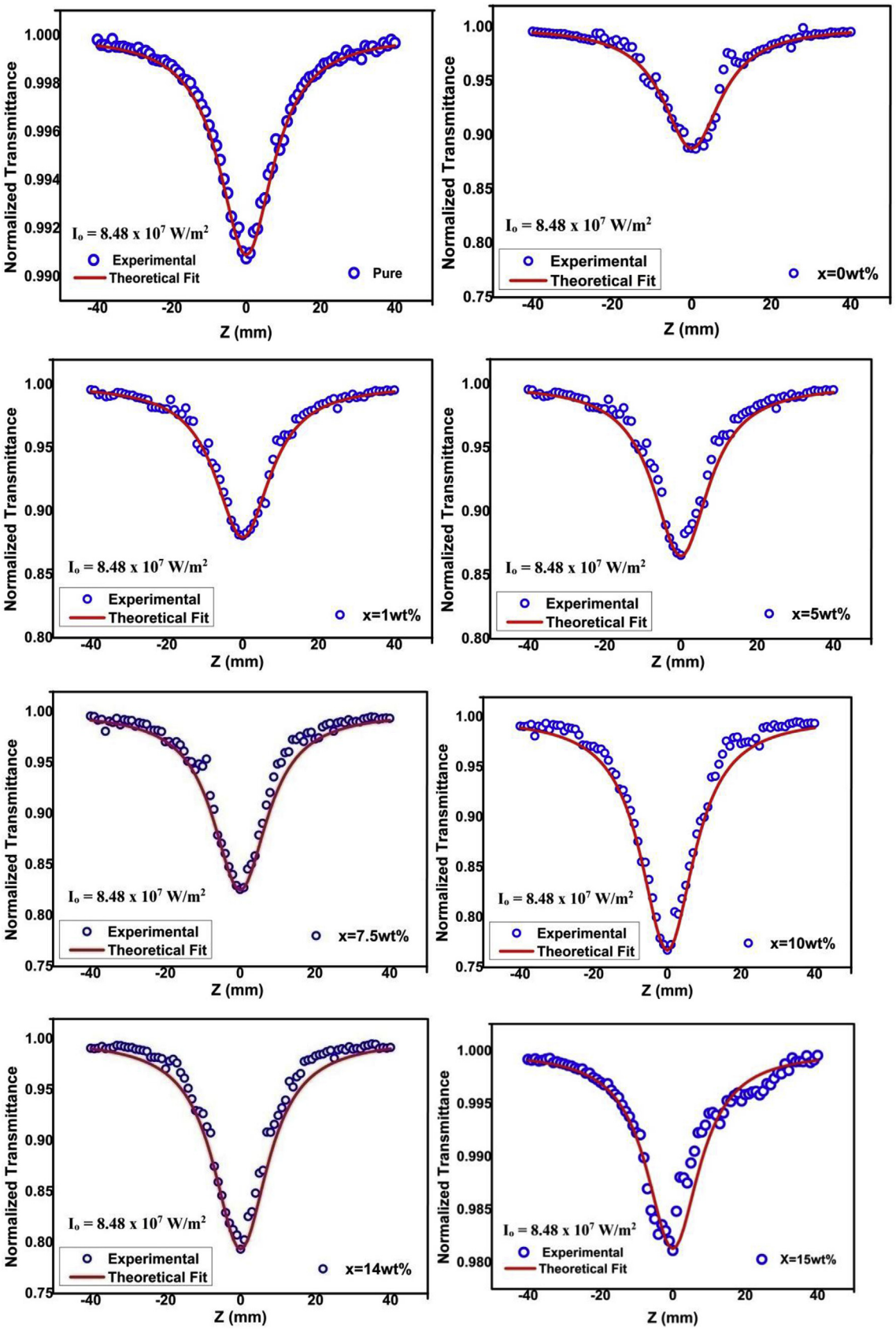

Fig. 16. Open-aperture Z-Scan traces for PVA nanocomposites.

Table 4
Third-order NLO parameters of PVA/(x) TiO_2 (15-x) CuO nanocomposites for x = 0, 1, 5, 7.5, 10, 14 and 15 wt% filling concentration.

Dopant Concentration	Non-linear absorption Coefficient (β) cm/W	Non-linear refractive Index (n_2) cm^2/W	Real part of Non-linear optical susceptibility ($\chi_R^{(3)}$) esu	Imaginary part of Non-linear optical susceptibility ($\chi_{img}^{(3)}$) esu	N (Third order Non-linear optical susceptibility (χ^3) esu
Pure PVA	3.19×10^{-5}	-1.57×10^{-9}	8.97×10^{-8}	7.72×10^{-9}	9.01×10^{-8}
0 wt%	3.94×10^{-4}	-1.94×10^{-8}	1.10×10^{-6}	9.51×10^{-8}	1.12×10^{-6}
1 wt%	4.24×10^{-4}	-2.04×10^{-8}	1.16×10^{-6}	1.02×10^{-7}	1.17×10^{-6}
5 wt%	4.74×10^{-4}	-2.15×10^{-8}	1.22×10^{-6}	1.14×10^{-7}	1.23×10^{-6}
7.5 wt%	6.14×10^{-4}	$- 2.20 \times 10^{-8}$	1.25×10^{-6}	1.48×10^{-7}	1.26×10^{-6}
10 wt%	8.17×10^{-4}	-2.56×10^{-8}	1.46×10^{-6}	1.98×10^{-7}	1.48×10^{-6}
14 wt%	7.24×10^{-4}	-2.35×10^{-8}	1.34×10^{-6}	1.74×10^{-7}	1.35×10^{-6}
15 wt%	3.26×10^{-4}	-1.38×10^{-8}	7.89×10^{-6}	7.87×10^{-8}	7.93×10^{-7}

the main cause for the reduction of dielectric constant at a relatively higher frequency. The same behaviour is shown in Fig. 8 regarding the decrease in dielectric loss (ε'') with increase in frequency. The dielectric loss at low frequency is observed high because of the mobile charge carriers present in the polymer chain. At high frequencies rapid motion is necessary for the dipole to adjust with faster field variations, which leads to a lag in the accomplishment of the equilibrium in an electric field [39]. Thus lag in the response of diploes with applied electric field experiences a process known as dielectric relaxation leading to dielectric loss. The dielectric loss factor (tan δ) is expressed in terms of real and imaginary parts of dielectric constant as, $\tan\delta = \frac{\varepsilon''}{\varepsilon'}$. Fig. 9 signifies the dependence of dielectric loss factor with frequency for prepared nanocomposites. Out of all prepared nanocomposites, for x = 10 wt% filling concentration the maximum real dielectric constant of 7.5 is observed for frequency 3×10^3 Hz.

3.5. AC conductivity

The frequency dependence of electrical behaviour of materials is [40],

$$\sigma_{ac} = \sigma_{dc} + \sigma_1(\omega) \quad (1)$$

$$\text{or } \sigma_{ac} = \sigma_{dc} + A\omega^n \quad (2)$$

Where, σ_{dc} stands for frequency independent DC conductivity, $\sigma_1(\omega)$ is usually consigned to the hopping conduction, A is pre-exponential factor which dependence on temperature, n is the exponent (n < 1 the hopping motion is translational one while n > 1 the motion is localized one). From the aforementioned law, the AC conductivity are affected by the subsequent factors like, Electrode effect (active low frequencies), DC plateau (at intermediate frequencies) and defect process (which can be explained by the term $A\omega^n$). The enhancement in AC electrical conductivity up to filling concentration x = 10 wt%. On the other hand, increase in conductivity with frequency characterises ω^n (n is the exponential) is also observed. The Jonscher power law is applied for all the prepared composites and confirm by non-linear fit. Initially, for all the nanocomposites slight deviation is observed at lower frequencies. From the non-linear fit, the obtained value of n < 1 indicates to diffusion limit. The transport mechanism is predicated by the hopping process among the two sites separated by an energy barrier.

Apart from these, AC conductivity of prepared PVA nanocomposites is calculated using the relation $\sigma_{AC} = 2\pi f \varepsilon_0 \varepsilon''$. Where f is the applied frequency of ac, ε'' is the dielectric loss and ε_0 is the permittivity of free space. Fig. 10 gives the common fashion of increasing conductivity of nanocomposites for different filling concentrations with the rise in frequencies. It is also observed that for x = 10 wt% the conductivity is high. With rising in frequency the polar bond of PVA/(x)TiO_2(15-x)CuO nanocomposites rotates and causing the dielectric transition. This will change the chemical composition of the PVA main chain unit due to the formation of charge transport complexes. This in turn makes the nanocomposites chains more flexible and hence enhances the electrical conductivity [41,42]. The rise in doping concentration makes the conductive nanoparticles appears to inter-mingle each other establishing a continuous network for transportation of electrons. The higher filing concentration of TiO_2 nanoparticles can induce the higher crystalline region in the sample and, accordingly, hinders the ion immigration. Further, in the percolation threshold, (x = 10 wt %) a small rise in the concentration of Nanofiller possibly will intensify the bridges in the conducting network. Hence, the rise in the concentration of Nanofiller also enhances the conducting domains leading to a monotonic rise in conductivity [43–45].

3.6. UV–visible spectroscopy studies

Absorption and optical energy gap measurement of unfilled and PVA/(x)TiO_2(15-x)CuO for x = 0, 1, 5, 7.5, 10, 14 and 15 wt% filling concentration PVA nanocomposites were carried out using JASCO V-630 UV–Visible spectrophotometer in the wavelength range of 100–900 nm. Figs. 11 and 12 explore the UV–Visible spectra of pure PVA and filled PVA nanocomposites. PVA absorbs strongly in the wavelength range of 200–400 nm and same is simulated as a shoulder like a band at 269 nm in Fig. 11. Fig. 12 discloses the redshift correspondingly to the wavelength from 300 nm to 561 nm having different absorption intensities. The transferral in absorption bands and band edges is owing to the creation of inter/intermolecular H-bonding of nanoparticles with the OH groups of the PVA nanocomposites main chain.

The optical energy gaps from the UV–visible spectra are obtained by transmuting the continuums into Tauc's plots by means of the frequency dependent absorption coefficient as given by Mott and Devis [46,47]. Fig. 13 gives the optical energy gap of pure PVA and Fig. 14 gives the optical energy gap of PVA/(x) TiO_2 (15-x) CuO for x = 0, 1, 5, 7.5, 10, 14 and 15 wt% filling concentration. Table 3 exposes the decrease in the energy gap with rising in filling concentration from x = 0 wt% to x = 10 wt%. The low energy gap (1.44eV) of PVA nanocomposites reveals their applications in optoelectronic devices [48,49]. At the optimum concentration x = 10 wt%, the PVA starts to form interpenetrating polymer chain with added Nano filler. Throughout the cross-linking process, the PVA main chains are covalently fused to the added Nano filler which encourages chain rigidity. Thus interpenetrating random coils of PVA results, deceased segmental motion or molecular mobility to form a complex conformation. These factors increase the crystallinity thereby lessening in the energy gap [50–52].

3.7. Photoluminescence

Fig. 15 shows an image of photoluminescence (PL) of PVA/(x)TiO_2(15-x)CuO nanocomposites with x = 0, 1, 5, 7.5, 10, 14 and 15 wt% filling concentration using F2700 spectrophotometer. PL is an operative technique which determines the electronic structure be influenced by the particle size [53,54]. The PL measurements of prepared nanocomposites were performed at room temperature at an excitation wavelength of 370 nm. The nanocomposites spectacle exciting peaks at 380 nm and precise strong emission bands in the visible range at 680 nm by neglecting the reflection occurred by a different order of harmonics [55,56]. The emission band at 380 nm corresponds to the

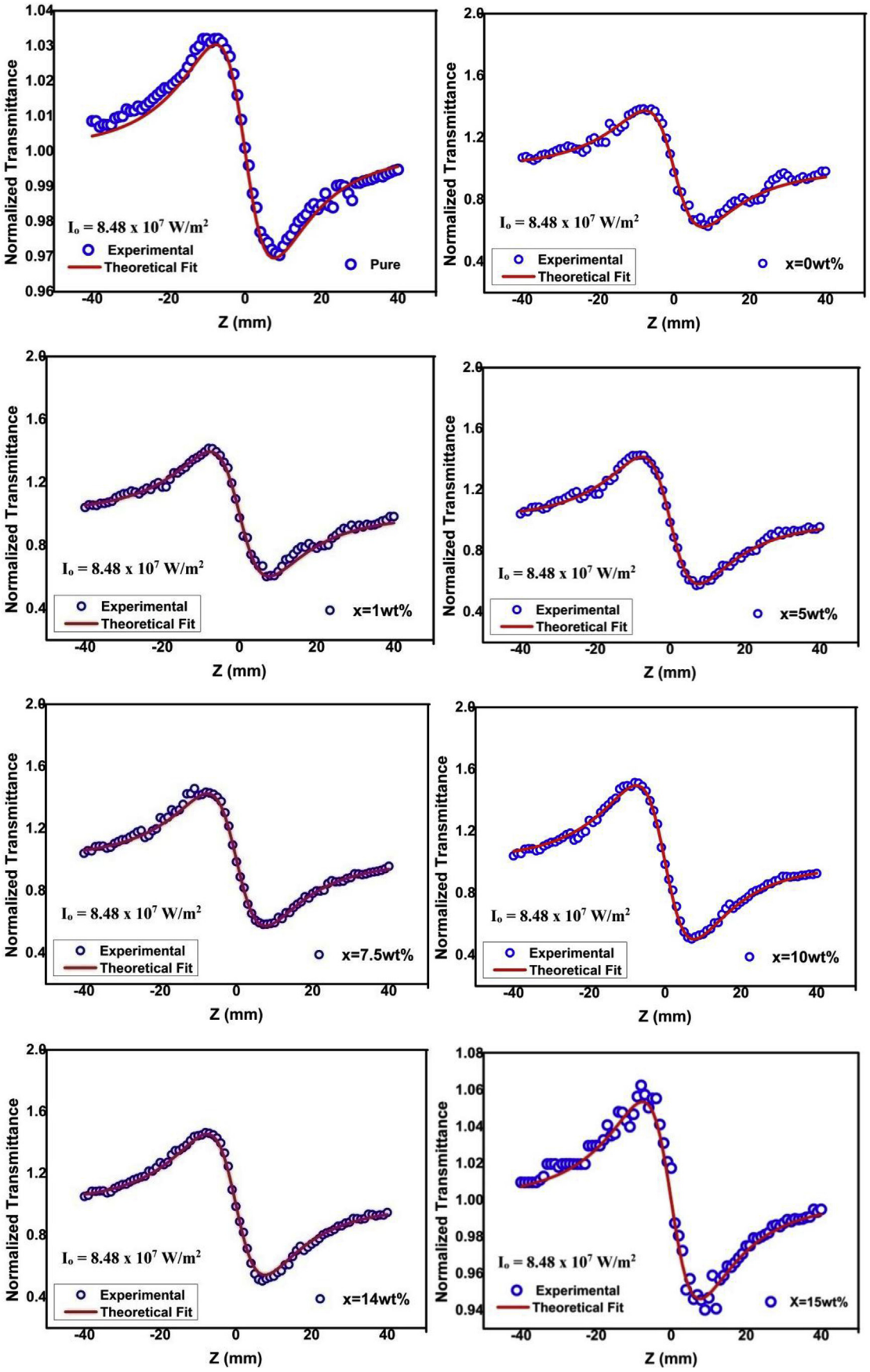

Fig. 17. Closed-aperture Z-Scan plots for PVA nanocomposites.

surface trap induced effects and intense emission band at 680 nm resemble the electron-hole recombination of TiO_2 and CuO nanoparticles.

3.8. Nonlinear absorption (NLA) and nonlinear refractive index (NRI)

Third order nonlinear optical features such as nonlinear absorption coefficient (β), nonlinear refractive index (n_2) and third order nonlinear optical susceptibility (χ^3) of PVA/(x) TiO_2 (15-x) CuO nanocomposites with x = 0, 1, 5, 7.5, 10, 14 and 15 wt% filling concentration were investigated by the means of Z-scan scan technique with DPSS continuous wave laser having 532 nm wavelength and 200 mW output power. To investigate nonlinear absorption coefficient of filled nanocomposites, open aperture (OA) Z-scan measurements were carried out and the same is presented in Fig. 16. During the exposure the sample cell is placed at Z = 0 position and was moved to and fro along the z-axis and at each Z position input beam energy, transmitted beam energy and their ratio were measured. All the nanocomposites show transmittance valley in open aperture scan and direct strong reverse saturation absorption. Using the relation, $T_{open} = 1 - \frac{\beta I_o L_{eff}}{2\sqrt{2}\left[1+\frac{Z^2}{Z_o^2}\right]}$, two photon absorption coefficient (β) was calculated. Where $Z_o = \frac{\pi\omega_o^2}{\lambda}$ is the beam waist, $L_{eff} = [\frac{1-\exp^{-\alpha_o' d}}{2\,\alpha_o'}]$ is the effective thickness of the sample, α_o' is the linear absorption coefficient,d the sample length and I_0 is the laser beam intensity [57]. The third order nonlinear absorption coefficient of the prepared nanocomposites increases with an increase in filling concentration from x = 0 wt% to x = 10 wt% and is shown in Table 4.

Closed aperture (CA) Z-scan technique is used to measure the nonlinear refractive index (n_2) of the nanocomposites [58]. In closed aperture Z scan technique the aperture is kept in front of the detector for all prepared nanocomposites and the results are shown in Fig. 17. Theoretical fitting of experimental CA data, the phase shift ($\Delta\phi_o$) of the PVA filled composites are determined using the following equation, $(Z) = 1 - \frac{4X\Delta\phi_o}{(X^2+1)(X^2+9)}$, where $x = z/z_o$and using $\Delta\phi_o = Kn_2 I_o L_{eff}$, the nonlinear refractive index (n_2) is evaluated. χ(3) (Third order nonlinear optical susceptibility) is attained by means of the equation, $|\chi^{(3)}| = |Re\chi^{(3)} + Im\chi^{(3)}|$. Where $Re\,\chi^{(3)} = 2C\,n_2\varepsilon_o n_o^2$ exemplifies the real part of third-order NLO susceptibility and $Im\,\chi^{(3)} = \frac{C\,\varepsilon_o\,\lambda\,\beta\,n_o^2}{2\,\pi}$ epitomizes the imaginary part of the third-order NLO susceptibility. The results of the third-order NLO properties of the filled PVA nanocomposites are presented in Table 4. The observed enhancement behaviour is due to the strong complex formation of OH group of PVA matrix with the added nano fillers. This enhances the crystallinity, surface roughness and also the carrier concentration of the prepared filled samples. Apart from these, the nonlinear refractive index (n_2) of closed aperture fluctuates with the concentration of loaded Nanofillers due to the difference in the nonlinear phase shift. These induced factors make the PVA/(x) TiO_2(15-x)CuO nanocomposites with x = 0, 1, 5, 7.5, 10, 14 and 15 wt % filling concentration to retain outstanding NRI (n_2) when matched to other testified materials of similar interest. These prepared PVA composites find appropriate uses in optical based switches.

4. Conclusion

Inorganic polymer nanocomposites PVA/(x)TiO_2(15-x)CuO with x = 0, 1, 5, 7.5, 10, 14 and 15 wt% filling concentration are prepared by ex-situ and solvent casting routes and investigated their structural, electrical, mechanical, dielectric, linear and nonlinear optical properties. The XRD spectra endorse the semi crystalline nature of the nanocomposites for the loaded x = 10 wt% optimized filler concentrations. UV–Vis spectroscopy reveals the reduction in optical energy gap from x = 0 wt%to x = 10 wt% filling concentration. AFM authorizes the uniform grain structures of pure PVA and changes in surface morphology with added nanocomposites. IV analysis recommend a high conductivity of $\sigma_{dc} = 3.21 \times 10^{-8} Scm^{-1}$for x = 10 wt% optimum filling concentration. The UTM shows high tensile strength of 48.36 MPa devouring Young's modulus of 1685.70 MPa. Photoluminescence studies spectacles a maximum intensity for x = 10 wt%. Dielectric studies disclosures the maximum real dielectric constant value of 7.5 for the frequency 3×10^3 Hz of loaded concentration at x = 10 wt%. Third order NLO studies using Z scan technique shows excellent susceptibility of the third order Non-linear optical susceptibility of 1.48×10^{-6} esu and refractive index of $2.56 \times 10^{-8}\,cm^{-2}/W$ for x = 10 wt% filling concentration finding its use in nonlinear optical devices.

Declaration of interests

The authors declare that they have no known competing financial interests or personal relationships that could have appeared to influence the work reported in this paper.

Acknowledgement

The authors thank Dr. Sangappa, Department of Physics, Mangalore University, Karnataka, India for valuable support in providing the UTM. Author also thanks Dr. Rekha P.D., Yenopoya Research Centre, Yenepoya University, Mangalore, Karnataka, India, for providing the F2700 PL spectrophotometer.

References

[1] J. Osuntokun, P.A. Ajibade, Physica B 496 (2016) 106–112.
[2] M.B. Mohamed, Z.K. Heiba, J. Mater. Sci. Mater. Electron. 28 (2017) 17578–17586.
[3] E.L.S. Karimat, M.B. Mohamed, Z.K. Heiba, A.R. Al-Nabriss, Superlattice. Microst. 75 (2014) 311–323.
[4] Y.S. Tamgadge, A.L. Sunatkari, S.S. Talwatkar, V.G. Pahurkar, G.G. Muley, Opt. Mater. 51 (2016) 175–184.
[5] N.B. Rithin Kumar, Crasta Vincent, B.M. Praveen, Mohan Kumar, Nanotechnol. Rev. 4 (2015) 457–467.
[6] P.C. Patel, S. Ghosh, P.C. Srivastava, Physica 93 (2017) 148–152.
[7] Shujahadeen B. Aziza, Rawezh B. Marif, M.A. Brza, Amir N. Hassan, Hiwa A. Ahmad, Younis A. Faidhalla, M.F.Z. Kadir, Results in Physics 13 (2019) 102220.
[8] N. Rajeswari, S. Selvasekarapandian, S. Karthikeyan, C. Sanjeeviraja, Y. Iwai, Kawamura, J Ionics 19 (2013) 1105–1113.
[9] N.B.R. Kumar, V. Crasta, B.M. Praveen, Mater. Res. Express 3 (2016) 055012.
[10] Shujahadeen B. Aziz, Hameed M. Ahmed, Ahang M. Hussein, Awder B. Fathulla, Rawaz M. Wsw, Rekawt T. Hussein, J. Mater. Sci. Mater. Electron. DOI 10.1007/s10854-015-3457-6.
[11] J.S. Cruz, G.T. Delgado, R.C. Perez, S.J. Sandoval, O.J. Sandoval, C.I.Z. Romero, J.M. Marin, O.Z. Angel, Thin Solid Films 493 (2005) 83–87.
[12] S.B.B. Wang, C.H.H. Hsiao, S.J.J. Chang, K.T.T. Lam, K.H.H. Wen, S.C.C. Hung, et al., Sens. Actuators, A 171 (2011) 207–218.
[13] M.M. Rahman, aJ. Saleh Ahammad, J.-H. Jin, S.J. Ahn, J.-J. Lee, Sensors 10 (2010) 4855–4886.
[14] Z. Yang, Xiuli He, L. Jianping, Z. Huigang, G. Xiaoguang, Sensors 128 (2007) 293–298.
[15] R. Kumar, Y. Diamant, A. Gedanken, Chem. Mater. 12 (2000) 2301–2305.
[16] N.G. Imam, M.B. Mohamed, Superlattice. Microst. 73 (2014) 203–213.
[17] Y.-H. Choi, D.-H. Kim, H.S. Han, S. Shin, S.-H. Hong, K.S. Hong, Langmuir 30 (2014) 700–709.
[18] Y.N. Chang, M. Zhang, L. Xia, J. Zhang, G. Xing, Materials 5 (2012) 2850–2871.
[19] H. Taoda, Res. Chem. Intermed. 34 (2008) 417–426.
[20] A.L. Manoj, V. Shaji, S.N. Santhosh, Catalysts 2 (2012) 572–601.
[21] F. Motta, A. Strini, E. Carraro, S. Bonetta, Amb. Express 3 (2013) 1–8.
[22] K. Doushita, T. Awahara, J. Sol. Gel Sci. Technol. 22 (2001) 91–98.
[23] E.Y. Oliveira, R. Bode, M.V. Escárcega-Bobadilla, G. Maier, New J. Chem. 40 (2016) 4625–4634.
[24] Shujahadeen B. Aziz, Nanomaterials 7 (2017) 444.
[25] M. Abdelaziz, E.M. Abdelrazek, Physica B 390 (2007) 1–9.
[26] N.B. Rithin Kumar, Crasta Vincent, Rajashekar F. Bhajantri, B.M. Praveen, Journal of Polymers (2014) 7. Article ID 846140.
[27] B. Gananatha Shetty, Crasta Vincent, N.B. Rithin Kumar, K. Rajesh, Raghavendra Bairy, Mater. Res. Express 6 (2019) 7.
[28] Ziquan Liu, Ruming Wang, Fangjun Kan, Fuyi Jiang, Asian J. Chem. 26 (3) (2014) 655–659.
[29] M. Shipra, E. Gupta, T. Manoj, Chin. Sci. Bull. 56 (2011) 1639–1657.
[30] H. Park, H.I. Kim, G.H. Moon, W. Choi, Energy Environ. Sci. 9 (2016) 411–433.
[31] Z. Yang, W. Zhang, A. Liu, S. Tang, J. Solid State Chem. 180 (2007) 1390–1396.
[32] J.W. Zhu, D. Li, X.J. Yang, L.D. Lu, X. Wang, Mater. Lett. 58 (2004) 3324–3327.
[33] Pedro Henrique Cury Camargo, Kestur Gundappa Satyanarayana,

Fernando Wypych, Mater. Res. 12 (1) (2009) 1–39.
[34] Suman Mahendia, A.K. Tomar, Shyam Kumar, Mater. Sci. Eng. B 176 (2011) 530–534.
[35] R.F. Bhajantri, V. Ravindrachary, A. Harisha, C. Ranganathaiah, G.N. Kumaraswamy, Appl. Phys. A 87 (2007) 797–805.
[36] D. Mardare, G.I. Rusu, J. Optoelectron. Adv. Mater. 6 (2004) 333–336.
[37] V. Rao, P.V. Ashokan, M.H. Shridhar, Mater. Sci. Eng. A 281 (2000) 213–220.
[38] Kiesow, J.E. Morris, C. Radehaus, A. Heilmann, J. Appl. Phys. 94 (2003) 6988–6990.
[39] C.S. Ramya, T. Savitha, S. Selvasekarapandian, G. Hirankumar, Ionics 11 (2005) 436–441.
[40] N.B.R. Kumar, V. Crasta, B.M. Praveen, B. Gananatha Shetty, Bull. Mater. Sci. 42 (2019) 124.
[41] R.F. Bhajanti, V. Ravindrachary, A. Harisha, G. Ranganathaiah, G.N. Kumaraswamy, Appl. Phys. A 87 (2007) 797–805.
[42] M.H. Harun, E. Saion, A. Kassim, E. Mahmud, M.Y. Hussain, I.S. Mustafa, J. Adv.Sci. Arts 1 (2009) 9–16.
[43] C.U. Devi, A.K. Sharma, V.V.R.N. Rao, Mater. Lett. 56 (2002) 167–174.
[44] Kiesow, J.E. Morris, C. Radehaus, A. Heillman, J. Appl. Phys. 94 (2003) 6988–6990.
[45] Shujahadeen B. Aziz, Ranjdar M. Abdullah, Electrochim. Acta 285 (2018) 30–46.
[46] N.F. Mott, E.A. Devis, Electronic Process in Non-crystalline Materials, second ed., Oxford University Press, Oxford, UK, 1979.
[47] J. Tauc, Optical properties of solids, in: F. Abeles (Ed.), In Optical Properties of Solid, North-Holland, Amsterdam, The Netherlands, 1972, p. 277.
[48] Shujahadeen B. Aziz, Rebar T. Abdulwahid, Hazhar A. Rsaul, Hameed M. Ahmed, J. Mater. Sci. Mater. Electron. DOI 10.1007/s10854-016-4278-y.
[49] Shujahadeen B. Aziza, Mariwan A. Rasheed, Ahang M. Hussein, Hameed M. Ahmed, Mater. Sci. Semicond. Process. 71 (2017) 197–203.
[50] E.J. Shin, Y.H. Lee, S.C. Choi, J. Appl. Polym. Sci. 91 (2004) 2407–2415.
[51] N.B. Rithin Kumar, Crasta Vincent, B.M. Praveen, Physics Research International (2014) 1–9. Article ID 742378,.
[52] Shujahadeen B. Aziz, Aso Q. Hassan, Sewara J. Mohammed, Wrya O. Karim, M.F.Z. Kadir, H.A. Tajuddin, N.N.M.Y. Chan, Nanomaterials 9 (2019) 216.
[53] Z.K. Heiba, M.B. Mohamed, N.G. Imam, J. Mol. Struct. 1136 (2017) 321–329.
[54] M. Ramrakhiani, S. Sahare, Solid State Phenom. 201 (2013) 181–196.
[55] Z.K. Heiba, M.B. Mohamed, N.G. Imam, J. Inorg, Organomet.Polym.Mater. 26 (2016) 780–787.
[56] D.V. Thai, P.V. Ben, T.M. Thi, N.V. Truong, H.H. Thu, Opt. Quant. Electron. 48 (2016) 362.
[57] L. Irimpan, V.P.N. Nampoori, P. Radhakrishnan, J. Mater. Res. 23 (2008) 2836–2845.
[58] D.M. Jundale, S.T. Navale, G.D. Khuspe, D.S. Dalavi, J. Mater. Sci. Mater. Electron. 24 (2013) 3526–3536.